Tensor meson production in proton-proton collisions from the color glass condensate

François Fillion-Gourdeau* and Sangyong Jeon†
Department of Physics, McGill University, 3600 University Street, Montreal, Canada H3A 2T8
(Received 3 October 2007; published 2 May 2008)

We compute the inclusive cross section of f_2 tensor-meson production in proton-proton collisions at high energy. We use an effective theory inspired from the tensor-meson dominance hypothesis that couples gluons to f_2 mesons. We compute the differential cross section in the $k_\perp$ factorization and in the color glass condensate formalism in the low density regime. We show that the two formalisms are equivalent for this specific observable. Finally, we study the phenomenology of f_2 mesons by comparing theoretical predictions of different parametrizations of the unintegrated gluon distribution function. We find that f_2-meson production is another observable that can be used to put constraints on these distributions.

DOI: 10.1103/PhysRevC.77.055201 PACS number(s): 13.85.Ni, 24.85.+p, 12.38.Mh

I. INTRODUCTION

High-energy hadronic collisions are complex phenomena that combine many-particles physics and quantum chromodynamics (QCD). Making predictions for the production of particles in these reactions involves the understanding of both hadron wave function and processes of particle creation. Many advances have been made in the past few decades in those areas through the application of perturbative QCD (pQCD) to the description of experimental data. The pQCD analysis relies generally on factorization schemes such as the collinear factorization and the $k_\perp$ factorization. Different procedures are implemented in these approaches to improve the perturbative expansion by resumming infrared divergences. Many observables are well described by QCD factorizations. For example, $k_\perp$ factorization was used successfully to compute heavy-quarks production in proton-antiproton collisions [1–9] while collinear factorization is one of the main computational tools for deep inelastic scattering and for a number of other applications [10,11]. The main difference between the two formalisms is their range of validity. The $k_\perp$ factorization is used to describe semihard processes characterized by the typical momentum transfer μ obeying $\Lambda^2_{\rm QCD} \ll \mu^2 \ll s$ (where $\Lambda_{\rm QCD}$ is the QCD scale and $\sqrt{s}$ is the center-of-mass energy) while collinear factorization is used to describe hard processes with $\Lambda^2_{\rm QCD} \ll \mu^2 \sim s$.

Some time ago, new ideas were developed to take into account effects due to the recombination of gluons in nuclei at very high energy (or small-x) [12–16]. These saturation effects introduce a new scale called the saturation scale Q_s at which the probability of gluon recombination becomes important. A naive estimate of Q_s shows that it depends on the momentum fraction (x) and the number of nucleon (A) in such a way that $Q_s^2 \sim A^\delta x^{-\lambda}$ [14,15]. The exponents δ and λ can be determined from experiments and theoretical calculations. At small enough x or large enough A, the saturation scale becomes hard ($Q_s^2 \gg \Lambda^2_{\rm QCD}$) and weak coupling techniques can be used. The color glass condensate (CGC) formalism includes these saturation effects in a semiclassical way [12–16]. More precisely, it resums the large order contributions coming from the gluon cascades in the regime where $\Lambda^2_{\rm QCD} \ll \mu^2 \leqslant Q_s^2 \ll s$. In proton-proton ($pp$) collisions at Relativistic Heavy Ion Collider (RHIC) energy (with $Q_s < \mu$), saturation can be neglected and collinear or $k_\perp$ factorization can be used in the calculation of observables. It is interesting to compare the predictions of CGC and factorizations in that regime. For heavy-quark production [17] and gluon production [18,19], the CGC in the low density limit and $k_\perp$ factorization are equivalent in pp collisions. We show in this article that this also holds true for tensor-meson production.

In this study, we focus on the production of $f_2(1270)$, the lightest spin-2 meson. It is a bound state of light quarks (u or d) and antiquarks. It has a mass of 1.27 GeV, a decay width of 185 MeV, and quantum numbers of $I^G(J^{PC}) = 0^+(2^{++})$ [20]. This particle was studied in the past using different methods such as the chiral perturbation theory [21–23] and the effective field theory method [24]. Another approach is to use the tensor-meson dominance (TMD) hypothesis, where one assumes that the energy-momentum tensor form factor are dominated by the exchange of a f_2 meson. The idea of TMD was first applied to phenomenology by Renner [25,26] to describe the tensor-meson exchange channel in pion-nucleon scattering. This idea was then used in many other applications [27–35]. Borrowing ideas from the TMD hypothesis, namely the coupling of spin-2 mesons to the energy-momentum tensor of strongly interacting matter (including quarks, gluons and hadrons), we show how the inclusive cross section of f_2 mesons can be computed in proton-proton collisions at RHIC and at the large hadron collider (LHC). This type of coupling is used in Ref. [34] and in Ref. [36] for the computation of the f_2 decay rate into photons and pions. In Ref. [36], the authors compute successfully (within experimental error) the decay rate of f_2 into two photons using AdS/QCD. To obtain this result, they must include both the gluon and quark contributions to the energy-momentum tensor. In this article, we consider only the gluonic part of the energy-momentum tensor because the hadrons in high-energy collisions interact mostly through gluons. More precisely, we study the process where the interaction of two gluons coming from different nuclei interact and produce one on-shell f_2

*ffillion@hep.physics.mcgill.ca
†jeon@physics.mcgill.ca

meson because this should be the dominant process at high energy.

We consider only the case of pp collisions and discuss briefly the case of proton-nucleus (pA) collisions. For nucleus-nucleus (AA) collisions, the total number of f_2 mesons produced should be important but most of them cannot be detected because they will decay inside the medium created by the collision. This can be seen as follows. Our analysis shows that tensor mesons are created during the first instants of the collision ($t < 1$ fm/c), when the system is still out of equilibrium and well described by strong classical fields. RHIC data indicate that from about 1 to 10 fm/c, a thermalized medium exists. The mean lifetime of f_2 mesons is about 1.1 fm/c, which is smaller than the lifetime of the medium. Moreover, the probability that these particles can travel longer than the size of the system is very small unless their momenta satisfy $|\mathbf{k}| \gg M$. This is unlikely at the RHIC energy because the f_2 mesons are created by small-x gluons, which have rather small longitudinal momenta. Thus, the f_2 mesons created in AA collisions would mostly decay inside the medium and their decay products rescatter, losing correlation. In that sense, most tensor mesons produced should be unobservable in AA collisions unless they are produced at the surface. This can be seen experimentally in the invariant mass distribution where the f_2 signal is essentially nonexistent [37]. This is not the case for pp and pA because no medium is created and the particles obtained from f_2 decay can escape without rescattering. For these reasons, our present analysis can be applied only to pp and pA collisions.

This article is organized as follow. Section II is dedicated to the statement of the spin-2 tensor-meson effective theory. We use an effective free Lagrangian describing spin-2 particles dynamics that is similar to Kaluza-Klein modes in extradimensions studies. The f_2 interacts with strongly interacting matter through the energy-momentum tensor. In Sec. III, the computation of the cross section at leading order in perturbation theory using $k_\perp$ factorization is performed. The process considered is the tree-level interaction of two gluons giving one f_2. In Sec. IV, the same calculation is done using the CGC. We start by deriving a reduction formula relating the cross-section production to a correlator of energy-momentum tensors that can be evaluated using the CGC formalism. We use the solution of the gauge field in covariant gauge at leading order in the color charge densities to evaluate the cross section. The two formalisms are then compared and shown to be equivalent in the limit of low densities (dilute systems). In both cases, the production cross section is related to the unintegrated gluon distribution functions of the two protons. Section V is devoted to the phenomenology of f_2-meson production at RHIC. In that section, the predictions of standard parametrizations of the unintegrated distribution function are compared.

Throughout the article, we use both light-cone coordinates defined by

$$p^+ = \frac{p^0 + p^3}{\sqrt{2}}; \quad p^- = \frac{p^0 - p^3}{\sqrt{2}} \tag{1}$$

and Minkowski coordinates. We also use the metric convention $\eta_{\mu\nu} = (1, -1, -1, -1)$.

II. EFFECTIVE THEORY

In our approach, the tensor meson couples to the rest of the strongly interacting matter through the energy-momentum tensor. The energy-momentum tensor is a conserved current that has the same quantum numbers as tensor mesons, so a coupling of this type is natural. The effective interaction Lagrangian describing the interaction of gluons, quarks, and hadrons with tensor mesons is given by [34,36]

$$\mathcal{L}_{\text{int}}(x) = \frac{1}{\kappa} f_{\mu\nu}(x) T^{\mu\nu}_{\text{gluons}}(x) + \frac{1}{\kappa_{\text{q}}} f_{\mu\nu}(x) T^{\mu\nu}_{\text{quarks}}(x) + \frac{1}{\kappa_{\text{h}}} f_{\mu\nu}(x) T^{\mu\nu}_{\text{hadrons}}(x), \tag{2}$$

where $f_{\mu\nu}$ is the symmetric spin-2 tensor field; κ and $\kappa_{\text{q,h}}$ are the coupling constants; and $T^{\mu\nu}_{\text{gluons,quarks,hadrons}}$ are the energy-momentum tensors of gluons, quarks, and hadrons, respectively. This type of interaction preserves all the symmetries of the matter Lagrangian by construction. For simplicity, we consider only one species of tensor meson, namely $f_2(1270)$. Generalization to include other species such as the $f_2'(1525)$ is straightforward. Note also that in this theory, the coupling constants κ and $\kappa_{\text{q,h}}$ are free dimensionful (dimension of energy) parameters that need to be fixed by experiments. It is possible to fix their value by assuming that they are the same ($\kappa = \kappa_{\text{q}} = \kappa_{\text{h}}$). Within this assumption, the hadronic and partonic sectors of the theory couple to tensor mesons in the same way. Then, κ can be fixed using the f_2 pions decay data and one finds that $\kappa \approx 0.1$ GeV [30,34,36]. The approach favored in this article differs from this because we do not assume that the coupling constants are the same, that is $\kappa \neq \kappa_{\text{q}} \neq \kappa_{\text{h}}$. The value of the coupling will be evaluated by comparing our results with experiments (see the last section for a comparison with STAR data).

For a physically consistent formulation of f_2 tensor Lagrangian, we borrow from recent developments of Kaluza-Klein theory and write the following free Lagrangian describing spin-2 particles dynamics [38,39]

$$\mathcal{L}_{\text{free}}(x) = -\tfrac{1}{2} f^{\mu\nu}(x)(\partial^2 + M^2) f_{\mu\nu}(x) + \tfrac{1}{2} f^{\rho}_{\rho}(x)(\partial^2 + M^2) f^{\sigma}_{\sigma}(x) - f^{\mu\nu}(x)\partial_\mu\partial_\nu f^{\rho}_{\rho}(x) + f^{\mu\nu}(x)\partial_\mu\partial_\sigma f^{\sigma}_{\nu}(x). \tag{3}$$

The first term of the Lagrangian is the usual kinetic term while the other terms are necessary to have the right number of degrees of freedom. This will be discussed in more details in Sec. IV A.

This Lagrangian describes a low-energy effective theory for tensor-meson dynamics. Therefore, its domain of validity is restricted to a certain energy domain which is of the order of the mass of f_2 mesons because it is the only scale appearing in the problem. Although this cannot be proven rigorously, the results obtained from this theory should be taken with caution at very high transverse momenta.

In high-energy proton-proton collisions, it is well-known from parton distribution functions that gluons dominate the cross section, so the main contribution to f_2 production comes from the gluonic sector of the theory. The energy-momentum tensor of gluons can be obtained from the Yang-Mills

Lagrangian by varying the metric. It is given by

$$T^{\mu\nu}_{\text{gluons}}(x) = \tfrac{1}{4} g^{\mu\nu} G_{\sigma\rho a}(x) G_a^{\sigma\rho}(x) - G^{\mu}_{\sigma a}(x) G_a^{\sigma\nu}(x), \quad (4)$$

where

$$G^{\mu\nu}_a(x) = \partial^\mu A^\nu_a(x) - \partial^\nu A^\mu_a(x) + g f_{abc} A^\mu_b(x) A^\nu_c(x) \quad (5)$$

is the usual field-strength tensor and A^μ_a is the gauge field of gluons with color index a. The Feynman rules associated with this Lagrangian are presented in Appendix A. This effective theory can now be used to compute the cross section of f_2 production in high-energy pp collisions.

III. f_2-MESON PRODUCTION CROSS SECTION FROM PQCD

In this section, the f_2-meson cross section in pp collisions is evaluated in the $k_\perp$-factorization formalism. This formalism can be used when the collision is semihard, meaning that $\Lambda^2_{\text{QCD}} \ll \mu^2 \ll s$, where $\sqrt{s}$ is the center-of-mass energy, $\Lambda_{\text{QCD}} \sim 200$ MeV is the usual QCD scale, and μ is the typical parton interaction scale. The parton interaction scale is related to the transverse mass of the produced particles $\mu^2 \sim M^2_\perp \equiv M^2 + k^2_\perp$.

One of the most important point for the validity of the present approach is the existence of a hard scale. It guarantees that the semihard inequality described above is satisfied at small tranverse momentum. In our case, this scale is the mass of f_2 given by $M = 1.27$ GeV. Clearly, for large-enough transverse momentum, it is possible to use $k_\perp$ factorization because we have $\Lambda^2_{\text{QCD}} \ll \mu^2 \ll s$. At very small transverse momentum, this inequality is only marginally satisfied ($\frac{\mu^2}{\Lambda^2_{\text{QCD}}} \approx 30$), so it is not certain that $k_\perp$ factorization is a good approximation in that regime. In this article, we look at the whole range of transverse momentum for f_2 production. For very small transverse momentum $|k_\perp| < 2$–3 GeV, the f_2 production spectra should be regarded as an extrapolation of the perturbative result to a region where $k_\perp$ factorization cannot be rigorously proven.

In that sense, the f_2's observed at RHIC and LHC should be produced from semihard processes, unless they are measured at transverse momentum of the order of the center-of-mass energy ($|k_\perp| \sim \sqrt{s}$). Moreover, these processes occur at small-x ($x \approx M^2_\perp/s \ll 1$), where the collinear factorized perturbation theory is spoiled because of logarithmic terms like $[\ln(\mu^2/\Lambda^2_{\text{QCD}})\alpha_s]^n$, $[\ln(\mu^2/\Lambda^2_{\text{QCD}})\ln(1/x)\alpha_s]^n$ and $[\ln(1/x)\alpha_s]^n$ [1–4]. The essence of $k_\perp$ factorization is to resum these "large-logs," leading to a description in terms of the unintegrated gluon distribution functions $\phi(x, k_\perp, \mu^2)$. These functions give the probability to find a gluon with longitudinal momentum x and transverse momentum $k_\perp$ at the scale μ^2 [1,2].

Although $k_\perp$ factorization has not been proven rigorously for f_2 production, it is, however, analogous to the heavy-quark production studied in Refs. [1,2] and to Higgs production studied in Ref. [8]. Moreover, as shown in Sec. IV, the CGC can be used to justify this approach because the two formalisms give the same cross section. This is similar to the work described in Ref. [17], where it is shown how to recover $k_\perp$ factorization from the CGC formalism. For these reasons, using $k_\perp$ factorization for f_2 production at RHIC and LHC energies is justified.

A. Cross section in $k_\perp$ factorization

The inclusive cross section in the $k_\perp$-factorization formalism is given by [6–8]

$$(2\pi)^3 2E_k \frac{d\sigma^{pp\to f_2 X}}{d^3k} = 16\pi^2 \int_0^1 \frac{dx_1}{x_1}\frac{dx_2}{x_2} \int \frac{d^2q_\perp d^2p_\perp}{(2\pi)^4} \phi_1(x_1, p^2_\perp, \mu^2) \times \phi_2(x_2, q^2_\perp, \mu^2)\,(2\pi)^3 2E_k \frac{d\sigma^{g^*g^*\to f_2 X}}{d^3k}, \quad (6)$$

where

$$(2\pi)^3 2E_k \frac{d\sigma^{g^*g^*\to f_2}}{d^3k} = \frac{1}{2\hat{s}} |\mathcal{M}^{g^*g^*\to f_2}|^2 (2\pi)^4 \delta^4(p+q-k) \quad (7)$$

is the high-energy limit of the cross section for off-shell gluons g^* to on-shell f_2, $\hat{s} = x_1 x_2 s$ is the $k_\perp$-factorization flux factor [1,2], $x_{1,2}$ are momentum fractions of the gluons and $\phi_{1,2}(x_{1,2}, k_\perp, \mu^2)$ are unintegrated gluon distribution functions of proton 1 and 2. The unintegrated distribution functions are related to the usual parton distribution functions of gluons (appearing in collinear factorization) by

$$\int_0^{\mu^2} dk^2_\perp \phi\left(x, k^2_\perp, \mu^2\right) \approx x g(x, \mu^2), \quad (8)$$

where $g(x, \mu^2)$ is the usual gluonic parton distribution function in collinear factorization.

B. Kinematics and matrix element

To compute the production cross section of f_2 mesons, the high-energy limit of the lowest-order matrix element between two off-shell gluons and one on-shell f_2 has to be calculated. The Feynman diagram included is shown in Fig. (1). It can be evaluated by using the Feynman rules presented in Appendix A. The main difference with usual pQCD calculation is in the average on polarization of off-shell gluons. In $k_\perp$

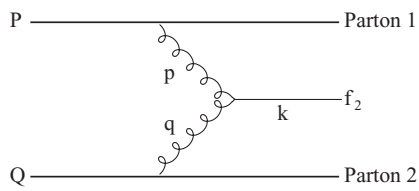

FIG. 1. Feynman diagram included in the lowest-order calculation of f_2 production in the $k_\perp$-factorization formalism. Two partons with momenta P and Q, each part of proton 1 and 2, emit two off-shell gluons with momenta p and q. The gluons combine to produce a f_2 meson with momentum k.

factorization, the polarization tensor obeys [1,2]

$$\sum_{\lambda} \epsilon_{\lambda}^{*\mu}(p)\epsilon_{\lambda}^{\nu}(p) = \frac{p_{\perp}^{\mu} p_{\perp}^{\nu}}{p_{\perp}^2}, \tag{9}$$

where $p_{\perp}^{\mu} \equiv (0, p_{\perp}, 0)$. The sum over polarizations differs from the usual result because we are considering off-shell gluons with a virtuality given by $p^2 = -p_{\perp}^2$. The exact form is due to the coupling of gluons to partons through eikonal vertices as well as gauge invariance and Ward identities [2].

In the center-of-mass frame, the four-momenta of protons moving in the $\pm z$ direction in Minkowski coordinates are

$$P = \left(\frac{\sqrt{s}}{2}, 0, 0, \frac{\sqrt{s}}{2}\right) \text{ and } Q = \left(\frac{\sqrt{s}}{2}, 0, 0, -\frac{\sqrt{s}}{2}\right). \tag{10}$$

The momenta of gluons in the large-energy limit ($|p_{\perp}|, |q_{\perp}| \ll \sqrt{s}$) are simply

$$p = \left(\frac{x_1\sqrt{s}}{2}, p_{\perp}, \frac{x_1\sqrt{s}}{2}\right) \text{ and } q = \left(\frac{x_2\sqrt{s}}{2}, q_{\perp}, -\frac{x_2\sqrt{s}}{2}\right). \tag{11}$$

The f_2 meson is on-shell and its momentum satisfies $k^2 = M^2$.

The matrix element for f_2 production is

$$\begin{aligned} &|\mathcal{M}^{g^*g^*\to f_2}|^2 \\ &\quad\equiv \frac{1}{\left(N_c^2-1\right)^2} \sum_{a,b} \sum_{\lambda,\lambda',\lambda''} |\mathcal{T}^{g^*g^*\to f_2}|^2 \\ &\quad= \sum_{a,b} \frac{1}{\left(N_c^2-1\right)^2} P_{\mu\nu\alpha\beta}(k) \frac{p_{\perp\rho} p_{\perp\eta}}{p_{\perp}^2} \frac{q_{\perp\sigma} q_{\perp\gamma}}{q_{\perp}^2} \\ &\qquad\times V_{ab}^{\mu\nu\rho\sigma}(k,q,p)\left[V_{ba}^{\alpha\beta\eta\gamma}(k,q,p)\right]^*, \end{aligned} \tag{12}$$

where a, b are color indices, N_c is the number of color, and $V_{ba}^{\alpha\beta\eta\gamma}(k,q,p)$ are vertices defined in Appendix A, and the spin-2 projection operator is defined as

$$\begin{aligned} P_{\mu\nu\rho\sigma}(k) &\equiv \sum_{\lambda} \left[\epsilon_{\mu\nu}^{\lambda}(k)\right]^* \epsilon_{\rho\sigma}^{\lambda}(k) \\ &= \left(\frac{1}{2}\hat{g}_{\mu\rho}\hat{g}_{\nu\sigma} + \frac{1}{2}\hat{g}_{\mu\sigma}\hat{g}_{\nu\rho} - \frac{1}{3}\hat{g}_{\mu\nu}\hat{g}_{\rho\sigma}\right)_k \end{aligned} \tag{13}$$

with $\hat{g}_{\mu\nu} = g_{\mu\nu} - k_{\mu}k_{\nu}/M^2$.

By working out the contractions, the above expression can be simplified further (with p^+ and q^- signifying the light-cone energies of partons) and it gives

$$\begin{aligned} &|\mathcal{M}^{g^*g^*\to f_2}|^2 \\ &= \frac{(p^+q^-)^2}{\left(N_c^2-1\right)\kappa^2} P_{\mu\nu\alpha\beta}(k) \frac{H_{\perp}^{\mu\nu}(p_{\perp},q_{\perp}) H_{\perp}^{\rho\sigma}(p_{\perp},q_{\perp})}{p_{\perp}^2 q_{\perp}^2}, \end{aligned} \tag{14}$$

where we defined $H_{\perp}^{\mu\nu}(p_{\perp}, q_{\perp})$ as

$$H_{\perp}^{11}(p_{\perp},q_{\perp}) = -H_{\perp}^{22}(p_{\perp},q_{\perp}) = q^1p^1 - q^2p^2, \tag{15}$$

$$H_{\perp}^{12}(p_{\perp},q_{\perp}) = H_{\perp}^{21}(p_{\perp},q_{\perp}) = q^1p^2 + q^2p^1. \tag{16}$$

All other components of $H_{\perp}^{\mu\nu}$ are zero.

C. Cross section

Once the matrix element is known, it is possible to evaluate the differential cross section. Using the kinematics [Eq. (11)] and the δ functions, the integrations over $x_{1,2}$ can be easily done. The $k_{\perp}$-factorized differential cross section is

$$\begin{aligned} &(2\pi)^3 2E_k \frac{d\sigma^{pp\to f_2X}}{d^3k} \\ &= 16\pi^4 \frac{P_{\mu\nu\alpha\beta}(k)}{\left(N_c^2-1\right)\kappa^2} \int \frac{d^2q_{\perp}d^2p_{\perp}}{(2\pi)^4} (2\pi)^2\delta^2(p_{\perp}+q_{\perp}-k_{\perp}) \\ &\quad\times \phi_1(x_+, p_{\perp}^2, \mu^2)\phi_2(x_-, q_{\perp}^2, \mu^2) \\ &\quad\times \frac{H_{\perp}^{\mu\nu}(p_{\perp},q_{\perp}) H_{\perp}^{\alpha\beta}(p_{\perp},q_{\perp})}{p_{\perp}^2 q_{\perp}^2}, \end{aligned} \tag{17}$$

where $x_{\pm} = \frac{1}{\sqrt{s}}[E_k \pm k_z]$. This is one of the major results of this article. It relates the production cross section of f_2 mesons to the unintegrated gluon distribution function. The phenomenology of this equation and its derivation from the CGC formalism are studied in the next sections.

D. Limit of collinear factorization

The procedure to recover collinear factorization cross sections from $k_{\perp}$ factorization is well known [1,6,7,17] and will serve as a consistency check for Eq. (17). The limit $|p_{\perp}|, |q_{\perp}| \to 0$ has to be taken in the matrix elements and the integration on the azimuthal angle has to be performed. The last step is to use the relation Eq. (8) to perform the last integral and relate the unintegrated distributions to the collinear distributions.

For the case of f_2 production, the integration on azimuthal angles of the $p_{\perp}, q_{\perp}$-dependent part of the matrix element is

$$\begin{aligned} &\int_0^{2\pi} d\theta_p d\theta_k \lim_{|p_{\perp}|,|q_{\perp}|\to 0} P_{\mu\nu\alpha\beta}(k) \frac{H_{\perp}^{\mu\nu}(p_{\perp},q_{\perp}) H_{\perp}^{\alpha\beta}(p_{\perp},q_{\perp})}{p_{\perp}^2 q_{\perp}^2} \\ &\quad= 8\pi^2. \end{aligned} \tag{18}$$

Combining this result with Eq. (8) and Eq. (17), the cross section becomes

$$\begin{aligned} &(2\pi)^3 2E_k \frac{d\sigma_{\text{coll.}}^{pp\to f_2X}}{d^3k} \\ &\quad= \frac{2\pi^2 M^2}{\left(N_c^2-1\right)\kappa^2 s} (2\pi)^2\delta^2(k_{\perp}) G(x_+,\mu^2) G(x_-,\mu^2), \end{aligned} \tag{19}$$

which is exactly the same as the expression computed in the collinear formalism in Appendix B [see Eq. (B6)]. Thus, Eq. (17) has the right collinear limit.

IV. PRODUCTION OF f_2 MESONS FROM THE CGC

In collisions at very high energies, the wave function of a nucleus is dominated by soft gluons (small-x where x is the momentum fraction). The CGC is a formalism that describes the dynamics of these degrees of freedom in the limit of the large center-of-mass energy. In this approach, hard partons that carry most of the longitudinal momentum, and soft gluons that

have a small longitudinal-momentum component, are treated differently. Hard partons act as sources for soft gluons and are no longer dynamical degrees of freedom. The occupation number of soft gluons is large because of the emission enhancement at small-x, hence classical field equations can be used to understand their dynamics (for reviews of CGC, see Refs. [14–16]).

In the CGC picture, computing a physical quantity involves two main steps. The first one is to solve for the gauge field using the classical Yang-Mills equation of motion

$$[D_\mu, F^{\mu\nu}(x)] = J^\nu(x), \tag{20}$$

where the current $J_a^\nu(x) = \delta^{\nu+}\,\delta(x^-)\,\rho_{1,a}\,(x_\perp) + \delta^{\nu-}\,\delta(x^+)\,\rho_{2,a}\,(x_\perp)$ represents random static sources localized on the light cone [14,15]. In that case, $\rho_{1,2}(x_\perp)$ are color charge densities in the transverse plane of protons 1 and 2, respectively. The next step is to take the average over the distribution of color charge densities in the nuclei with weight functionals $W_{1,2}[\rho_{1,2}]$ that include the dynamics of the sources. For any operator that depends on the color charge densities, either directly or via the classical gluon fields, this average can be written as

$$\langle\hat{O}\rangle = \int \mathcal{D}\rho_1\mathcal{D}\rho_2 O[\rho_1,\rho_2]W_1[x_1,\rho_1]W_2[x_2,\rho_2]. \tag{21}$$

Computing the weight functional is a highly nonperturbative procedure so it usually involves approximation based on physical modeling. In the limit of a large nuclei at not too small x (0.01–0.1), it can be approximated by the McLerran-Venugopalan (MV) model, which assumes that the partons are independent sources of color charge [12,13]. In pp collisions, these approximations fail and the MV model cannot be used. Thus, a more phenomenological approach based on unintegrated distribution functions is better suited and is used throughout this article.

One important ingredient is missing for the computation of f_2-meson production cross section. It is necessary to have a relation between the cross section and a correlator that can be evaluated using Eq. (21). This is done in the next section by deriving a reduction formula for our effective theory.

A. Reduction formula for the effective theory

The production of tensor mesons from the CGC can be calculated from a reduction formula derived from the Lagrangian Eq. (3). The first step is to compute the equation of motion of the tensor field $f_{\mu\nu}$ given as usually by $L_{\mu\nu}(x) \equiv \frac{\delta S}{\delta f^{\mu\nu}(x)} = 0$. By using L^μ_μ, $\partial^\mu L_{\mu\nu}$ and $\partial^\mu\partial^\nu L_{\mu\nu}$, it is possible to put constraints on $L_{\mu\nu}$ so that it looks like a Klein-Gordon equation (see Ref. [38] for details). This procedure is very similar to the case of a massive vector field described in Ref. [40]. The following equation of motion is obtained [note that for the simplicity of this derivation, we chose only the coupling to one type of particles so that the interaction Lagrangian looks like $\frac{1}{\kappa} f_{\mu\nu}(x)T^{\mu\nu}(x)$, the case with the Lagrangian given in Eq. (2) can be similarly dealt with]

$$(\partial^2 + M^2) f_{\mu\nu}(x) = \frac{1}{\kappa}\Theta_{\mu\nu}(x), \tag{22}$$

where

$$\Theta_{\mu\nu}(x) = T_{\mu\nu}(x) - \left(\frac{\partial_\mu\partial_\nu}{M^2} + g_{\mu\nu}\right)\frac{T^\rho_\rho(x)}{3}, \tag{23}$$

as well as the following two constraints:

$$\partial^\mu f_{\mu\nu}(x) = -\frac{\partial_\nu T^\rho_\rho(x)}{3M^2\kappa} \quad\text{and}\quad f^\rho_\rho(x) = -\frac{T^\rho_\rho(x)}{3M^2\kappa}. \tag{24}$$

These constraints ensure that five degrees of freedom in $f_{\mu\nu}$ are eliminated in a covariant way. Therefore, this group of equations describes a spin-2 field with only five propagating modes in the free-field limit. Note that the source term $\Theta_{\mu\nu}$ consistently satisfies

$$\Theta^\rho_\rho(x) = -\frac{1}{3M^2}(\partial^2 + M^2)T^\rho_\rho(x) \tag{25}$$

and

$$\partial^\mu\Theta_{\mu\nu}(x) = -\frac{1}{3M^2}(\partial^2 + M^2)\partial_\nu T^\rho_\rho(x). \tag{26}$$

These equations can also be interpreted as operator equations in the quantized theory. They determine the dynamics of the field operator in the Heisenberg representation. Because the equation of motion Eq. (22) is linear in $f_{\mu\nu}$, the general solution can be easily obtained. Taking the Fourier transform of space coordinates only, the solution of the field operator is given by

$$\hat{f}_{\mu\nu}(t,\mathbf{k}) = \hat{f}^{(0)}_{\mu\nu}(t,\mathbf{k}) + \frac{1}{\kappa}\int_{-\infty}^{\infty} dt' G_{\rm ret}(t-t',\mathbf{k})\,\hat{\Theta}_{\mu\nu}(t',\mathbf{k}), \tag{27}$$

where $\hat{f}^{(0)}_{\mu\nu}(t,\mathbf{x})$ satisfies the free field equation and the retarded Green function in the mixed t and $\mathbf{k}$ representation is

$$G_{\rm ret}(t,\mathbf{k}) = \frac{\sin(E_k t)}{E_k}\theta(t). \tag{28}$$

It can be easily shown in momentum space that the solution $f_{\mu\nu}$ obeys the constraints in Eq. (24). Therefore, this solution obeys the requirements of spin-2 particles and describes the right dynamics.

The inclusive cross section is related to the average number $\bar{n}$ of f_2 produced. In terms of creation and annihilation operators, $\bar{n}$ is given by

$$(2\pi)^3 2E_k\frac{d\bar{n}}{d^3k} = \sum_\lambda \langle{\rm init}|\left(\hat{a}^{\lambda\dagger}_{\mathbf{k}}\right)_{\rm out}\left(\hat{a}^{\lambda}_{\mathbf{k}}\right)_{\rm out}|{\rm init}\rangle\,, \tag{29}$$

where $\lambda = 0, \pm1, \pm2$ are the polarization of the spin-2 tensor field. Here $|{\rm init}\rangle$ specifies a quantum state at $t = -\infty$ and the subscript "out" specifies that the operator is to be evaluated at $t = \infty$. As $t \to \infty$, we expect that the density of particles will become low and the fields become asymptotic. We start by writing the annihilation operators in terms of the field (we take the wave function normalization to be $\mathcal{Z} = 1$)

$$\left(\hat{a}^\lambda_{\mathbf{k}}\right)_{\rm out} = \lim_{t\to\infty}\left[\epsilon^\lambda_{\mu\nu}(k)\right]^*\left[E_k\hat{f}^{\mu\nu}(t,\mathbf{k}) + i\,\partial_t\hat{f}^{\mu\nu}(t,\mathbf{k})\right], \tag{30}$$

where the polarization tensor $\epsilon^\lambda_{\mu\nu}$ is traceless and transverse and satisfies

$$\left(\epsilon^\lambda_{\mu\nu}(k)\right)^*\epsilon^{\mu\nu}_{\lambda'}(k) = \delta_{\lambda,\lambda'}. \tag{31}$$

The creation operator can be written down analogously. Using Eq. (27), we then get

$$\left(\hat{a}^{\lambda}_{\mathbf{k}}\right)_{\text{out}} = \lim_{t\to\infty}\left(\hat{a}^{\lambda}_{\mathbf{k}}e^{-iE_kt}\right)_{\text{free}} + \lim_{t\to\infty}\frac{i}{\kappa}\int_{-\infty}^{t}dt'e^{-iE_k(t-t')}\left(\epsilon^{\lambda}_{\mu\nu}(k)\right)^{*}\hat{\Theta}_{\mu\nu}(t',\mathbf{k}), \tag{32}$$

where we used Eq. (28) to get

$$i\dot{G}_{\text{ret}}(t,\mathbf{k}) + E_kG_{\text{ret}}(t,\mathbf{k}) = ie^{-iE_kt}\theta(t). \tag{33}$$

Here,

$$\left(\hat{a}^{\lambda}_{\mathbf{k}}e^{-iE_kt}\right)_{\text{free}} = \left[\epsilon^{\lambda}_{\mu\nu}(k)\right]^{*}\left[E_k\hat{f}^{(0)\mu\nu}(t,\mathbf{k}) + i\partial_t\hat{f}^{(0)\mu\nu}(t,\mathbf{k})\right] \tag{34}$$

describes the time evolution of the initial tensor-meson population. Equation (32) is a reduction formula for f_2 production. To simplify the analysis, it is assumed that the initial state contains no or little tensor mesons

$$\left(\hat{a}^{\lambda}_{\mathbf{k}}\right)_{\text{free}}|\text{init}\rangle = 0, \tag{35}$$

which is a reasonable assumption for high-energy hadronic collisions. The average number of f_2 produced is then simply

$$(2\pi)^3 2E_k\frac{d\bar{n}}{d^3k} = \frac{1}{\kappa^2}P^{\mu\nu\rho\sigma}(k)\langle\hat{\Theta}^{\dagger}_{\mu\nu}(k)\hat{\Theta}_{\rho\sigma}(k)\rangle, \tag{36}$$

where $\hat{\Theta}_{\rho\sigma}(k)$ is the Fourier transform of $\hat{\Theta}_{\rho\sigma}(x)$ evaluated at the tensor-meson on-shell momentum. The projection operator $P^{\mu\nu\rho\sigma}(k)$ is obtained by summing over polarizations and is given by Eq. (13). The angular brackets $\langle\hat{O}\rangle$ here indicate an expectation value of $\hat{O}$ in the initial state. Due to the presence of the projection operator in Eq. (36), the equation can be further simplified. The partial derivatives in $\hat{\Theta}_{\mu\nu}$ simply result in factors of $k_\mu k_\nu$ in the Fourier transform. This implies that in Eq. (36), those partial derivative terms do not contribute due to the transversality of the projection operator $[P^{\mu\nu\rho\sigma}(k)k_\mu = 0]$ when k is an on-shell momentum. Furthermore, because $P^{\mu\nu\rho\sigma}$ is made up of $\epsilon^{\lambda}_{\alpha\beta}$, it is also traceless in the sense that $P^{\mu\nu\rho\sigma}g_{\mu\nu} = P^{\mu\nu\rho\sigma}g_{\rho\sigma} = 0$. Hence the $g_{\mu\nu}$ term in $\hat{\Theta}_{\mu\nu}$ does not contribute to this momentum distribution either. By making these simplifications and by doing the same derivation with the interaction Lagrangian Eq. (2), the following simple result is obtained

$$(2\pi)^3 2E_k\frac{d\bar{n}}{d^3k} = \sum_{i,j}\frac{1}{\kappa_i\kappa_j}P^{\mu\nu\rho\sigma}(k)\langle\hat{T}^{\dagger}_{i,\mu\nu}(k)\hat{T}_{j,\rho\sigma}(k)\rangle, \tag{37}$$

where the indices are $i, j = \{\text{gluons, quarks, hadrons}\}$. This is the main result of this section. It relates the average number of f_2 mesons produced to a correlator of energy-momentum tensors. This correlator can then be evaluated using any analytical or numerical methods. The average $\langle\ldots\rangle$ depends on the system studied. Looking at a plasma in equilibrium, it could be computed using finite temperature field theory or the AdS/CFT correspondence. However, as argued in the Introduction, tensor mesons cannot be observed in AA collisions where the lifetime of the thermalized medium is longer than the lifetime of f_2 mesons. Therefore, these techniques are not pursued here because we study pp (or, eventually, pA) collisions where no medium is created. In high-energy hadronic collisions, the correlator can be evaluated using the CGC once $T^{\mu\nu}$ is expressed in terms of the sources $\rho_{1,2}$. This is done in the next section.

The result obtained so far is exact given the Lagrangian (3). The only assumptions introduced in the calculation are:

(i) There are no tensor mesons in the initial state
(ii) The tensor-meson content of $T^{\mu\nu}$ is ignored ($T^{\mu\nu}_{f_2} \approx 0$)
(iii) The tensor mesons can be produced on mass shell.

The first assumption is justified by the fact that in high-energy collisions, the number of tensor-meson component in a nucleus before the collision is negligible. The second assumption is more subtle as it does not appear explicitly in this calculation. If this assumption is not made, the energy-momentum tensor depends on $f_{\mu\nu}$ through the hadronic sector. This makes the equation of motion nonlinear, which is much harder to solve explicitly. In a high-energy collision, the cross section is dominated by gluons, so it is consistent to assume that $T^{\mu\nu}_{f_2} \ll T^{\mu\nu}_{\text{gluons}}$ as long as the f_2 mesons are produced in small quantities. Finally, the last assumption is that tensor meson can be produced on-shell so that their spectral density is $\rho(M^2) \sim \delta(p^2 - M^2)$. However, the f_2 meson is a resonance, so the spectral density should be reasonably given by a Breit-Wigner function $\rho(M^2) \sim \Gamma/[(p^2 - M^2)^2 + M^2\Gamma^2]$ where Γ is the decay width. Because $M^2 \gg \Gamma^2$, we expect that corrections due to the finite decay width can be neglected and that we can approximate $\rho(M^2) \sim \Gamma/[(p^2 - M^2)^2 + M^2\Gamma^2] \sim \delta(p^2 - M^2)$.

Having expressed the average number of f_2 produced in terms of a correlator of energy-momentum tensors, it is possible to compute the cross section in the CGC formalism. In high-energy collisions, we have that $T^{\mu\nu}_{\text{gluons}} \gg T^{\mu\nu}_{\text{quarks}}, T^{\mu\nu}_{\text{hadrons}}$ so we can neglect the quark and hadronic contributions. Thus, in the CGC, the inclusive cross section for f_2 production is given by [17,41]

$$\begin{aligned}(2\pi)^3 2E_k\frac{d\sigma}{d^3k} &= \int d^2b_\perp(2\pi)^3 2E_k\frac{d\bar{n}(b_\perp)}{d^3k}\\ &= \frac{1}{\kappa^2}P_{\mu\nu\rho\sigma}(k)\int d^2b_\perp\int\mathcal{D}\rho_1\mathcal{D}\rho_2T^{\dagger\mu\nu}_{\text{gluons}}[\rho_1,\rho_2]\\ &\quad\times T^{\rho\sigma}_{\text{gluons}}[\rho_1,\rho_2]W_1[\rho_1]W_2[\rho_2;b_\perp],\end{aligned} \tag{38}$$

where $b_\perp$ is the impact parameter. The energy-momentum tensor $T^{\mu\nu}_{\text{gluons}}$ is a functional of the source through the classical gauge fields [see Eqs. (4) and (5) for the expression of the energy-momentum tensor as a function of the gauge field]. From now on, we drop the subscript in the energy-momentum tensor and we set $T^{\mu\nu} \equiv T^{\mu\nu}_{\text{gluons}}$.

B. Calculation of the cross section and relation to $k_\perp$ factorization

In this section, Eq. (38) is evaluated explicitly to leading order for pp collisions. The expansion parameters in a dilute system like a proton are the weak color charge densities

obeying $\rho_{1,2}/k_\perp^2 \ll 1$. The first step is to solve the Yang-Mills equation. In a full solution, the gauge field would be a functional in all orders of the color charge densities. However, because the sources are weak (or equivalently, if the typical transverse momentum is large [16,42]), the solution can be truncated and the calculation can be done analytically. The solution of Yang-Mills equation to first order in $\rho_{1,2}/k_\perp^2$ was found in covariant gauge $[\partial_\mu A_a^\mu(x) = 0]$ in Refs. [17, 19]. It is given by $A^\mu(k) = A_1^\mu(k) + A_2^\mu(k) + A_{12}^\mu(k)$, where $A_1^\mu(k)$, $A_2^\mu(k)$ are $O(\rho_1)$ and $O(\rho_2)$, respectively, but $A_{12}^\mu(k)$ is $O(\rho_1\rho_2)$. The explicit components of the gauge field are

$$A_{1,a}^+(k) = 2\pi\delta(k^-)\frac{\rho_{1,a}(k_\perp)}{k_\perp^2}, \tag{39}$$

$$A_{2,a}^-(k) = 2\pi\delta(k^+)\frac{\rho_{2,a}(k_\perp)}{k_\perp^2}. \tag{40}$$

All the other components are zero. The field A_{12}^μ gives a higher-order contribution to the energy-momentum tensor correlator $\langle T^{\dagger\mu\nu}(k)T^{\rho\sigma}(k)\rangle$, so it is not considered here. The leading-order contribution to the energy-momentum tensor correlator is $O(\rho_1^2\rho_2^2)$ and that can come only from different combinations of A_1^μ and A_2^μ. A term containing A_{12}^μ is at least $O(\rho_1^3\rho_2^2)$ or $O(\rho_1^2\rho_2^3)$. In principle, terms of $O(\rho_1^4)$, $O(\rho_2^4)$, $O(\rho_1\rho_2^3)$, and $O(\rho_1^3\rho_2)$ can also be included but they do not contribute to the cross section. They vanish when applying the projection operator $P^{\mu\nu\rho\sigma}(k)$ defined in Eq. (13). This is because the only nonvanishing components of $O(\rho_1^4)$, $O(\rho_2^4)$, $O(\rho_1\rho_2^3)$, and $O(\rho_1^3\rho_2)$ are $T^{++}T^{\pm\pm} \propto \delta(k^-)$ and $T^{--}T^{-\mp} \propto \delta(k^+)$. These are contracted with the components $P^{---\mp}(k)$ and $P^{+++\pm}(k)$ and this cancels using the fact that the metric components $g^{\pm\pm} = 0$ and $k^\pm\delta(k^\pm) = 0$. Finally, the non-Abelian part of the energy-momentum tensor can also be neglected because it gives contributions of at least $O(\rho_1^3\rho_2^2)$ or $O(\rho_1^2\rho_2^3)$. In summary, the leading-order contribution of the energy-momentum tensor correlator in a dilute system is given by the Abelian part of the energy-momentum tensor computed with at least two gauge fields A_1^μ's and two A_2^μ's.

The Abelian part of the energy-momentum tensor in momentum space is

$$\begin{aligned} T^{\mu\nu}(k) = \int \frac{d^4p}{(2\pi)^4}\Big\{ & \frac{1}{2}g^{\mu\nu}\big[-p_\alpha(k-p)^\alpha A_{\beta,a}(p)A_a^\beta(k-p) \\ & + p_\alpha(k-p)^\beta A_{\beta,a}(p)A_a^\alpha(k-p)\big] \\ & + p_\alpha(k-p)^\alpha A_a^\mu(p)A_a^\nu(k-p) \\ & - p_\alpha(k-p)^\nu A_a^\mu(p)A_a^\alpha(k-p) \\ & - p^\mu(k-p)^\alpha A_{\alpha,a}(p)A_a^\nu(k-p) \\ & + p^\mu(k-p)^\nu A_{\alpha,a}(p)A_a^\alpha(k-p)\Big\}. \end{aligned} \tag{41}$$

According to our previous discussion, the computation of $\langle T^{\dagger\mu\nu}(k)T^{\rho\sigma}(k)\rangle$ at leading order involves the evaluation of correlators with four gauge fields that have the following general form

$$\begin{aligned} \int \frac{d^4pd^4q}{(2\pi)^8} f^{\mu\nu\rho\sigma}_{\mu'\nu'\rho'\sigma'}(p,k,q)\big\langle & A_{s_1,a}^{\dagger\mu'}(p)A_{s_2,a}^{\dagger\nu'}(k-p) \\ & \times A_{s_3,b}^{\rho'}(q)A_{s_4,b}^{\sigma'}(k-q)\big\rangle, \end{aligned} \tag{42}$$

where $s_i = 1$ or 2 (and there is at least 2 of each type) and $f^{\mu\nu\rho\sigma}_{\mu'\nu'\rho'\sigma'}(p,k,q)$ is a function whose value is determined by the Lorentz indices structure and the momentum factors appearing in front of the fields inside the expression of $T^{\mu\nu}(k)$. We need to evaluate the correlator

$$\begin{aligned} & A^{\mu\nu\rho\sigma}_{s_1,s_2,s_3,s_4}(k,p,q) \\ & \quad \equiv \big\langle A_{s_1,a}^{\dagger\mu}(p)A_{s_2,a}^{\dagger\nu}(k-p)A_{s_3,b}^{\rho}(q)A_{s_4,b}^{\sigma}(k-q)\big\rangle \end{aligned} \tag{43}$$

for all values of s_i using the expressions of the gauge field in Eqs. (39) and (40). To leading order in $\rho_{1,2}$, they are given by

$$\begin{aligned} & A^{\mu\nu\rho\sigma}_{1,2,1,2}(k,p,q) \\ & = \delta^{\mu+}\delta^{\nu-}\delta^{\rho+}\delta^{\sigma-}(2\pi)^4\delta(p^-)\delta(k^+-p^+)\delta(q^-)\delta(k^+-q^+) \\ & \quad \times \frac{\langle\rho_{1,a}^\dagger(p_\perp)\rho_{1,b}(q_\perp)\rangle}{p_\perp^2 q_\perp^2}\frac{\langle\rho_{2,a}^\dagger(k_\perp-p_\perp)\rho_{2,b}(k_\perp-q_\perp)\rangle}{(k_\perp-p_\perp)^2(k_\perp-q_\perp)^2}, \end{aligned} \tag{44}$$

$$\begin{aligned} & A^{\mu\nu\rho\sigma}_{1,2,2,1}(k,p,q) \\ & = \delta^{\mu+}\delta^{\nu-}\delta^{\rho-}\delta^{\sigma+}(2\pi)^4\delta(p^-)\delta(k^+-p^+)\delta(q^+)\delta(k^--q^-) \\ & \quad \times \frac{\langle\rho_{1,a}^\dagger(p_\perp)\rho_{1,b}(k_\perp-q_\perp)\rangle}{p_\perp^2(k_\perp-q_\perp)^2}\frac{\langle\rho_{2,a}^\dagger(k_\perp-p_\perp)\rho_{2,b}(q_\perp)\rangle}{q_\perp^2(k_\perp-p_\perp)^2}, \end{aligned} \tag{45}$$

$$\begin{aligned} & A^{\mu\nu\rho\sigma}_{2,1,2,1}(k,p,q) \\ & = \delta^{\mu-}\delta^{\nu+}\delta^{\rho-}\delta^{\sigma+}(2\pi)^4\delta(p^+)\delta(k^--p^-)\delta(q^+)\delta(k^--q^-) \\ & \quad \times \frac{\langle\rho_{1,a}^\dagger(k_\perp-p_\perp)\rho_{1,b}(k_\perp-q_\perp)\rangle}{(k_\perp-p_\perp)^2(k_\perp-q_\perp)^2}\frac{\langle\rho_{2,a}^\dagger(p_\perp)\rho_{2,b}(q_\perp)\rangle}{p_\perp^2 q_\perp^2}, \end{aligned} \tag{46}$$

$$\begin{aligned} & A^{\mu\nu\rho\sigma}_{2,1,1,2}(k,p,q) \\ & = \delta^{\mu-}\delta^{\nu+}\delta^{\rho+}\delta^{\sigma-}(2\pi)^4\delta(p^+)\delta(k^--p^-)\delta(q^-)\delta(k^+-q^+) \\ & \quad \times \frac{\langle\rho_{1,a}^\dagger(k_\perp-p_\perp)\rho_{1,b}(q_\perp)\rangle}{q_\perp^2(k_\perp-p_\perp)^2}\frac{\langle\rho_{2,a}^\dagger(p_\perp)\rho_{2,b}(k_\perp-q_\perp)\rangle}{p_\perp^2(k_\perp-q_\perp)^2}. \end{aligned} \tag{47}$$

The averages separate into the average over each proton because at this order there is no correlation between ρ_1 and ρ_2. The other possibilities such as $A_{1,1,2,2}$ and $A_{2,2,1,1}$ do not contribute because they give terms proportional to $\delta(k^\pm)\delta^2(k_\perp)$. Because $k^2 = M^2$, these δ functions have no support. From these expressions, we see clearly that the cross section is related to averages of the sources like Eq. (21). The averages can then be evaluated using any model available. However, it is convenient for phenomenological applications to first relate averages to unintegrated gluon distribution functions.

These averages can be related to the unintegrated distribution function of $k_\perp$ factorization as follows [43,44]

$$\begin{aligned} & \langle\rho_{1,a}^\dagger(p_\perp)\rho_{1,b}(q_\perp)\rangle \\ & \quad = \frac{4\pi^2\delta_{ab}}{(N_c^2-1)}\left(\frac{p_\perp+q_\perp}{2}\right)^2 \\ & \qquad \times \int d^2x_\perp e^{i(p_\perp-q_\perp)\cdot x_\perp}\frac{d\phi_1\left(\frac{p_\perp+q_\perp}{2}|x_\perp\right)}{d^2x_\perp} \end{aligned} \tag{48}$$

$$\langle \rho^{\dagger}_{2,a}(p_\perp)\rho_{2,b}(q_\perp)\rangle = \frac{4\pi^2\delta_{ab}}{(N_c^2-1)}\left(\frac{p_\perp+q_\perp}{2}\right)^2 \times \int d^2y_\perp e^{i(p_\perp-q_\perp)(y_\perp+b_\perp)}\frac{d\phi_2\left(\frac{p_\perp+q_\perp}{2}|y_\perp\right)}{d^2y_\perp}, \quad (49)$$

where $\frac{d\phi_{1,2}(p_\perp|x_\perp)}{d^2x_\perp}$ are the unintegrated gluon distribution functions per unit area. By definition, they are related to the unintegrated distribution functions by

$$\phi_{1,2}(p_\perp) = \int d^2y_\perp \frac{d\phi_{1,2}(p_\perp|y_\perp)}{d^2y_\perp}, \quad (50)$$

where the integration is on the transverse extent of the nuclei.

Combining all these results together, it is possible to compute the cross section. The integration on the impact factor $\int d^2b_\perp$ in the definition of the cross section gives a δ function $(2\pi)^2\delta^2(p_\perp - q_\perp)$ in the second source average Eq. (49). After a lengthy but straightforward calculation where we substitute Eqs. (44)–(47) in Eqs. (38) and (41), we find that the cross section is

$$(2\pi)^3 2E_k\frac{d\sigma^{pp\to f_2X}}{d^3k} = 16\pi^4\frac{P_{\mu\nu\alpha\beta}(k)}{(N_c^2-1)\kappa^2}\int\frac{d^2q_\perp d^2p_\perp}{(2\pi)^4}(2\pi)^2\delta^2(p_\perp+q_\perp-k_\perp) \times \phi_1(p_\perp^2,\mu^2)\phi_2(q_\perp^2,\mu^2)\frac{H_\perp^{\mu\nu}(p_\perp,q_\perp)H_\perp^{\alpha\beta}(p_\perp,q_\perp)}{p_\perp^2 q_\perp^2}. \quad (51)$$

This has exactly the same structure as the cross section obtained in $k_\perp$-factorization shown in Eq. (17) but now it is derived as the low density limit of CGC. The longitudinal momentum fraction x dependence of the unintegrated distribution functions is introduced through quantum evolution. The weight functions $W_{1,2}[\rho_{1,2}]$ obeys a nonlinear evolution equation in x, the JIMWLK equation [45–48]. This makes the unintegrated gluon distribution function x dependent $\phi(q_\perp^2,\mu^2)\to\phi(x,q_\perp^2,\mu^2)$ and Eqs. (51) and (17) can be compared.

V. PHENOMENOLOGY FOR PROTON-PROTON COLLISIONS

Equation (51) [or Eq. (17)] can be used to study the phenomenology of f_2 production and to study different parametrizations of the unintegrated gluon distribution function. By contracting the indices of $P_{\mu\nu\alpha\beta}(k)H_\perp^{\mu\nu}(p_\perp,q_\perp)H_\perp^{\alpha\beta}(p_\perp,q_\perp)$, the cross section at midrapidity is given by

$$\left.\frac{d\sigma^{pp\to f_2X}}{d^2k_\perp dy}\right|_{y=0} = \frac{1}{2\pi(N_c^2-1)\kappa^2}\int d^2q_\perp d^2p_\perp\phi_1(x',p_\perp^2,\mu^2)\phi_2(x',q_\perp^2,\mu^2) \times \delta^2(k_\perp-p_\perp-q_\perp) \times\left\{1+\frac{k_\perp^2}{M^2}+\frac{\left[p_\perp^2(q_\perp\cdot k_\perp)+q_\perp^2(p_\perp\cdot k_\perp)\right]^2}{3M^4p_\perp^2q_\perp^2}\right\}, \quad (52)$$

where $x'=\sqrt{\frac{M^2+k_\perp^2}{s}}$. As can be seen in this expression, the precise measurement of the f_2 differential cross section is a direct probe of unintegrated distribution functions. Unintegrated distribution functions obey evolution equations like the Balitsky-Fadin-Kuraev-Lipatov (BFKL) or the Ciafaloni-Catani-Fiorani-Marchesini (CCFM) equations. Depending on the physical model used or the approximations involved in the solution of these equations, they can be parametrized in various ways. To get an estimate of f_2 production that can be compared with experimental data at RHIC, we use standard parametrizations [9][1]. The measurement of f_2 production can be used to put constraints on models of the unintegrated gluon distribution function by comparing the predictions of various approaches. In this article, we use the following parametrizations:

(i) DIG (derivative of the integrated gluon distribution function). By ignoring that the unintegrated distribution function depends on a factorization scale μ, it is possible to invert Eq. (8) to get

$$\phi_{\mathrm{DIG}}(x,p_\perp^2) = \left.\frac{dxg(x,\mu^2)}{d\mu^2}\right|_{\mu^2=p_\perp^2}, \quad (53)$$

where $xg(x,\mu^2)$ is the gluonic parton distribution function.

(ii) JB (J. Blumlein). The JB parametrization is based on a perturbative solution of the BFKL equation [9,49]. In this parametrization, the unintegrated gluon distribution function is written as

$$\phi_{JB}(x,p_\perp^2,\mu^2) = \int_x^1 dz\mathcal{G}(z,p_\perp,\mu^2)\frac{x}{z}g\left(\frac{x}{z},\mu^2\right), \quad (54)$$

where $g(x,\mu^2)$ is the collinear gluon distribution function and

$$\mathcal{G}(z,p_\perp^2,\mu^2) = \begin{cases}\frac{\bar\alpha_s}{zp_\perp^2}J_0\left[\sqrt{\bar\alpha_s\ln\left(\frac{1}{z}\right)\ln\left(\frac{\mu^2}{p_\perp^2}\right)}\right], & \text{if} \quad p_\perp^2\leqslant\mu^2\\ \frac{\bar\alpha_s}{zp_\perp^2}I_0\left[\sqrt{\bar\alpha_s\ln\left(\frac{1}{z}\right)\ln\left(\frac{p_\perp^2}{\mu^2}\right)}\right], & \text{if} \quad p_\perp^2>\mu^2.\end{cases} \quad (55)$$

In this last equation, J_0 and I_0 are the Bessel's and modified Bessel's functions of the first kind, respectively, and $\bar\alpha_s = 3\alpha_s/\pi$, where α_s is the strong coupling constant ($\alpha_s\approx 0.25$).

(iii) CCFM. The unintegrated gluon distribution function have been calculated numerically by solving the CCFM [50–52] evolution equations using a Monte Carlo method [53]. The initial conditions of the evolution

[1]We thank H. Jung for handing us his FORTRAN routine CAUNIGLU, which evaluates numerically all of these parametrizations. It can be found at http://www.desy.de/ jung/cascade/updf.html.

equation are determined from a fit of the proton structure function $F_2(x, Q^2)$. The result of this procedure for many data sets is implemented in the routine CAUNIGLU written by H. Jung.

(iv) KMR (Kimber-Martin-Ryskin). The KMR parametrization is obtained by solving an evolution equation similar to the CCFM equation. An approximate solution to this equation on the whole range of $p_\perp$ can be found by extrapolation. It leads to an unintegrated distribution function given by [9,54]

$$\phi_{\mathrm{KMR}}\left(x, p_\perp^2, \mu^2\right) = \begin{cases} \frac{xg(x,p_{\perp 0}^2)}{p_{\perp 0}^2} & \text{if} \quad p_\perp^2 < p_{\perp 0}^2 \\ \frac{\mathcal{G}_{\mathrm{KMR}}(x,p_\perp^2,\mu^2)}{p_\perp^2} & \text{if} \quad p_\perp^2 \geqslant p_{\perp 0}^2, \end{cases} \tag{56}$$

where the function $\mathcal{G}_{\mathrm{KMR}}(x, p_\perp^2, \mu^2)$ can be evaluated numerically and the nonperturbative part, for $p_\perp^2 < p_{\perp 0}^2 \sim 1\ \mathrm{GeV}^2$, is given by the MRST collinear distribution function.

For numerical computations, we set the number of color to $N_c = 3$, the center-of-mass energy to $\sqrt{s} \approx 200$ GeV (RHIC), and the mass of f_2 to 1.27 GeV. For the DIG parametrization, we use the GRV NLN collinear gluon distribution function and for the JB parametrization, we use the MRS collinear distribution. These choices are the default distribution functions implemented in the numerical routine. The numerical results of the differential cross section at midrapidity for seven different parametrizations at RHIC energy are presented in Fig. 2. In Fig. 3, we present the results for the $k_\perp$-integrated (for $0 < |k_\perp| < \sqrt{s}$) differential cross section for the CCFM parametrizations. All the numerical integrations are done with the CUBA package [55] using both CUHRE and VEGAS algorithms.

There are some qualitative differences between the predictions of the different unintegrated distribution functions. As shown in Fig. 2, the CCFM parametrizations decrease much faster at large $|k_\perp|$ than other parametrizations. At low $|k_\perp|$, the shape of the curves is different, especially the parametrization

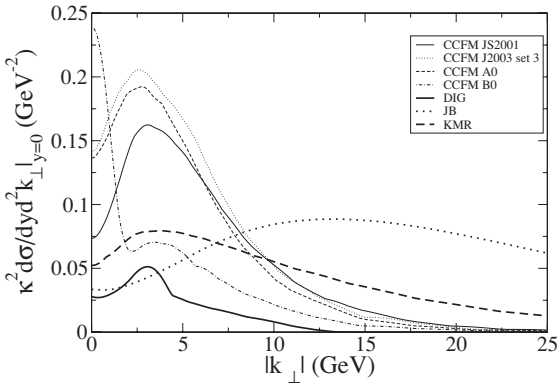

FIG. 2. Numerical results of the differential cross section as a function of transverse momentum $|k_\perp|$ for different parametrizations of the unintegrated distribution function at RHIC energy ($\sqrt{s} =$ 200 GeV). The results are shown for midrapidity ($y = 0$).

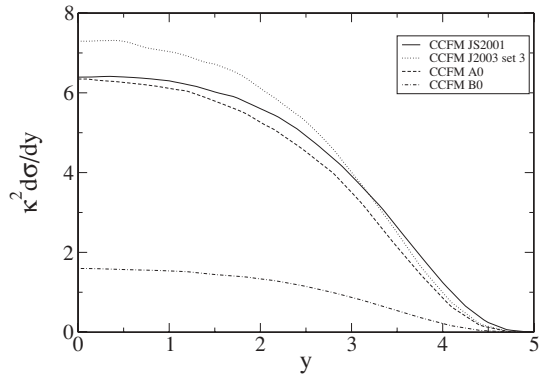

FIG. 3. Numerical results of the differential cross section as a function of rapidity y for the CCFM parametrizations of the unintegrated distribution function at RHIC energy ($\sqrt{s} = 200$ GeV). The transverse momentum $k_\perp$ has been integrated.

CCFM B0. These features give us a way to discriminate between the unintegrated distribution functions. As seen in Fig. 3, the parametrizations also lead to results that have different magnitudes. However, there is still an uncertainty on the overall magnitude because of the value of the coupling constant that have to be fixed by experiments. We now discuss this crucial point.

It is possible to compare our predictions to experimental data to fix the value of the coupling constant κ. The STAR collaboration has measured the production of f_2 mesons in the invariant mass spectrum of pions in proton-proton collisions at $\sqrt{s} \approx 200$ GeV and midrapidity [37]. The present data only show the invariant mass distribution in the transverse-momentum bin 0.6 GeV $< |k_\perp| <$ 0.8 GeV. From the graph presented in Ref. [37], it is possible to extract a rough estimate of the average number of f_2 produced per collision. Taking into account that the branching ratio of $f_2 \to \pi\pi$ is $\mathrm{BR}_{f_2\to\pi\pi} \approx 0.85$ [20], the average number of f_2 produced per collision is $\tilde{n} = \int_{-0.5}^{0.5} dy \int_{0.6\,\mathrm{GeV}}^{0.8\,\mathrm{GeV}} d^2k_\perp \frac{d\bar{n}}{d^2k_\perp dy} \approx 0.0024$. The total inelastic cross section for pp collisions at $\sqrt{s} = 200$ GeV is $\sigma_{\mathrm{inel}} \approx 40$ mb. Thus, we can convert the average multiplicity to a cross section and we get that

$$\tilde{\sigma} \approx \sigma_{\mathrm{inel}} \int_{-0.5}^{0.5} dy \int_{0.6\,\mathrm{GeV}}^{0.8\,\mathrm{GeV}} d^2k_\perp \frac{d\bar{n}}{d^2k_\perp dy} \approx 0.095\ \mathrm{mb\ (experimental)}. \tag{57}$$

This is an estimation of the experimental result for the f_2 production cross section.

We can then compute the integrated cross section $\tilde{\sigma}$ using Eq. (17). The results are presented in Table I. This can then be used to determine the value of the coupling constant κ and we find that depending on the parametrization used, κ is between 0.415 and 0.850 GeV. This is of the same order of magnitude but much larger than $\kappa \approx 0.1$ GeV obtained from pion decay by assuming a universal coupling of f_2 to the energy-momentum tensor of all strongly interacting particles [34,36] or by tensor-meson dominance [30]. This implies that the coupling of f_2 to gluons is much weaker than the

TABLE I. Numerical result for the total integrated cross section using different parameterization of the unintegrated distribution functions. To compare with STAR data, we integrated over 0.6 GeV $< |k_\perp| <$ 0.8 GeV and $-0.5 < y < 0.5$. From this result, it is possible to fix the value of the coupling constant κ.

Parameterization	$\kappa^2\tilde{\sigma}$	κ (GeV)
CCFM JS2001	0.0767	0.558
CCFM J2003 set 3	0.142	0.759
CCFM A0	0.134	0.737
CCFM B0	0.178	0.850
DIG	0.0424	0.415
JB	0.0578	0.484
KMR	0.0708	0.536

coupling to pions. There are three reasons that could explain this discrepancy. First, we are assuming that the f_2 meson can be produced as a stable on-shell particle. Strictly speaking, this is not the case because f_2 decays and form factors may need to be introduced. Second, there are no justifications *a priori* that the partonic sector should have the same coupling constant as that of the hadronic sector. In that sense, it is expected that the coupling of f_2 to gluons and hadrons will be different. Finally, we are neglecting hadronization, which can have a significant effect on the magnitude and shape of production spectra. Nevertheless, once the coupling constant is determined, all the curves presented in Fig. 2 and 3 become our predictions and can be compared to experimental data.

VI. CONCLUSION

Using our effective theory based on a coupling between the f_2 meson and the energy-momentum tensor, we were able to compute the inclusive cross section of f_2 tensor mesons in proton-proton collisions. This was done in the $k_\perp$-factorization formalism and in the CGC formalism. We showed that in the low density limit where the saturation effects does not have to be taken into account, the result of the calculation of the cross section in the CGC formalism reduces to the result of $k_\perp$ factorization. In some sense, we use the CGC to "prove" Eq. (6) for f_2 production. A rigorous treatment of factorization would involve a separation between the long- and short-distance dynamics using resummation and a reorganization of the perturbative expansion at all orders. Of course, this is a hard task to perform. In the CGC, the proof reduces solely to a power counting in the color charge densities. This kind of result was expected because it was shown in other explicit calculations, namely for gluon [18,19] and heavy-quark production [17].

We also looked into the phenomenology of f_2-meson production in proton-proton collisions at RHIC. We computed the differential cross sections for many different parametrizations of the unintegrated distribution function. We used STAR data to fix the coupling constant and found that it is larger than in other approaches, even if it has the same order of magnitude. These numerical results, although they should be supplemented by more experimental data, can be used for the determination of the most accurate unintegrated distribution function. This is very interesting because $k_\perp$ factorization is one of the main computational tools for particle production (like heavy quarks [1,2,5–7] and Higgs bosons [8]) in high-energy collisions at RHIC, LHC, and Tevatron. Having a consistent and precise unintegrated gluon distribution function is a crucial element in this formalism. Up to now, the main processes used to determine this distribution function were heavy quarks, dijets, and gauge bosons production in pp and electron-proton collisions [56]. Many improvements have been performed to fit experimental data from these distributions, but there are still many uncertainties, especially at small $k_\perp$. This uncertainty can also be seen in the variability of our numerical results for different parametrizations because they essentially lead to very different predictions. The f_2 production gives another observable that can be used to put constraints on the value of unintegrated distribution functions.

Throughout this analysis, we neglected hadronization that could have an effect on f_2 production spectra. This can be seen in pion production, for example, where some of these effects are taken into account in the fragmentation function [57–59]. The fragmentation function is dependent on the transverse momentum of the meson and, thus, it is important for the overall shape and magnitude of pion production spectra. In principle, these kinds of effects should also be taken into account in f_2-meson production but to the best of our knowledge, f_2 is usually not included in fragmentation functions. Moreover, there are not much experimental data that can be used to constrain f_2 hadronization models. For these reasons, as a first attempt to compute f_2 production, we use the effective theory described previously that leads to a simpler formulation but that should be a good estimation of the production processes. We are currently working on the inclusion of some hadronization effects in η' production, which is simpler than f_2 and for which the form factor and wave function were studied in the past. We will generalize these techniques to f_2 production in future work to have a quantitative estimate of hadronization effects.

Our work is also a starting point for further studies such as the production of f_2 in proton-nucleus collisions. According to the CGC picture, saturation effects should play an important role in such processes and, thus, the f_2 could be used to look for the initial state effects. In that sense, our calculation can serve as a point of comparison for the presence and the magnitude of these initial state effects. This is under investigation and should be the topic of a future publication.

ACKNOWLEDGMENTS

The authors thank F. Gelis, R. Venugopalan, T. Lappi, K. Tuchin, and J.-S. Gagnon for interesting and stimulating discussions. We thank especially Y. Kovchegov for clearing out some important aspects of the calculation. We also thank H. Jung for his help with the unintegrated distribution functions. This work was supported by the Natural Sciences and Engineering Research Council of Canada.

APPENDIX A: FEYNMAN RULES

In this appendix, the Feynman rules for gluon-f_2 interactions are presented. By referring to the interaction Lagrangian Eqs. (2), (4), and (5), it is easily seen that there are three possible interaction vertices: $gg \to f_2$, $ggg \to f_2$, and $gggg \to f_2$. However, the second and third ones are $O(g)$ and $O(g^2)$, respectively. They are not part of the leading-order contribution, so they are not considered in this analysis. The vertex $gg \to f_2$ can be evaluated and is given by

$$\begin{aligned} V_{ab}^{\mu\nu\rho\sigma}(k,p,q) &= \frac{i}{\kappa}(2\pi)^4\delta^4(-k+p+q)\delta_{ab}[g^{\mu\sigma}g^{\nu\rho}(q\cdot p) \\ &+ g^{\mu\rho}g^{\nu\sigma}(q\cdot p) - g^{\mu\nu}g^{\sigma\rho}(q\cdot p) \\ &- g^{\mu\sigma}q^\rho p^\nu - g^{\mu\rho}q^\nu p^\sigma - g^{\nu\rho}q^\mu p^\sigma - g^{\nu\sigma}q^\rho p^\mu \\ &+ g^{\rho\sigma}q^\mu p^\nu + g^{\rho\sigma}q^\nu p^\mu + g^{\mu\nu}q^\rho p^\sigma], \end{aligned} \tag{A1}$$

where $\kappa \approx O(100\ \text{MeV})$ is to be fixed by experiments. The vertex has the following important property:

$$p_\rho V_{ab}^{\mu\nu\rho\sigma}(k,p,q) = q_\sigma V_{ab}^{\mu\nu\rho\sigma}(k,p,q) = 0, \tag{A2}$$

which is related to the conservation of the Abelian part of the energy-momentum tensor. The external f_2 has the polarization $\epsilon_{\mu\nu}^\lambda(k)$. The f_2 Feynman propagator is

$$G_{\mu\nu\rho\sigma}(p) = \frac{-iP_{\mu\nu\rho\sigma}(p)}{p^2 - M^2 + i\epsilon}, \tag{A3}$$

where $P_{\mu\nu\rho\sigma}(p)$ is the projection operator given by Eq. (13).

APPENDIX B: COLLINEAR FACTORIZED CROSS SECTION

The tensor-meson production from pp collisions is investigated in this appendix using the usual parton model (the collinear factorization formalism). This formalism can be used when $\Lambda_{\text{QCD}}^2 \ll \mu^2 \sim s$, where, again, s is the squared center-of-mass energy, $\Lambda_{\text{QCD}} \sim 200$ MeV is the usual QCD scale, and μ is the typical parton interaction scale. At RHIC or LHC energy, this inequality is recovered at very large transverse momentum, when $\mu^2 \approx M_\perp^2 \sim s$, which may not be physically observable. However, it is interesting to make the calculation using this method as a consistency check for the $k_\perp$-factorized formalism.

The cross section for f_2-meson production in the collinear factorization formalism is given by

$$\begin{aligned} &(2\pi)^3 2E_k \frac{d\sigma^{pp\to f_2X}}{d^3k} \\ &= \int_0^1 dx_1 dx_2 G^{p_1}(x_1,Q^2)G^{p_2}(x_2,Q^2)(2\pi)^3 2E_k \frac{d\sigma^{gg\to f_2}}{d^3k}, \end{aligned} \tag{B1}$$

where G^{p_1,p_2} are the gluon distribution function of the two protons, $x_{1,2}$ are the longitudinal-momentum fraction ($x \equiv \frac{p^+_{\text{parton}}}{p^+_{\text{hadron}}}$), and Q^2 is the factorization scale. The cross section for on-shell gluons to on-shell tensor meson ($gg \to f_2$) is

$$\begin{aligned} &(2\pi)^3 2E_k \frac{d\sigma^{gg\to f_2}}{d^3k} \\ &= \frac{1}{4|p\cdot q|}|\mathcal{M}^{gg\to f_2}|^2(2\pi)^4\delta^4(k-p-q), \end{aligned} \tag{B2}$$

where $\mathcal{M}^{gg\to f_2}$ is the matrix element for the process $gg \to f_2$ (see Fig. 1 and take on-shell gluons). The matrix element can be easily computed to lowest order from the Feynman rules described in Appendix A.

The matrix element squared is averaged over the degrees of freedom of the initial state and summed over the degrees of freedom of the final state. Once conservation of energy and momentum are used, it is given by

$$\begin{aligned} |\mathcal{M}^{gg\to f_2}|^2 &= \frac{1}{(N_c-1)^2}\sum_{a,b}\frac{1}{4}\sum_{\lambda,\lambda',\lambda''}|\mathcal{T}^{gg\to f_2}|^2 \\ &= \frac{M^4}{2(N_c^2-1)\kappa^2} \end{aligned} \tag{B3}$$

where λ, λ', and λ'' are the polarizations of the gluons and f_2 mesons. This is obtained using the fact that for on-shell gluons, the sum on polarization is

$$\sum_\lambda \epsilon_\mu(k)\epsilon_\nu^*(k) = -g_{\mu\nu} + \frac{n_\mu k_\nu + n_\nu k_\mu}{n\cdot k} + \frac{n^2 k_\mu k_\nu}{(n\cdot k)^2} \to -g_{\mu\nu}. \tag{B4}$$

The replacement of the sum over polarizations by $g_{\mu\nu}$ (as depicted in the second part of the equation) is possible only because of the property (A2) of the vertex. The sum over polarizations of f_2 mesons is given by Eq. (13).

The initial gluons do not have transverse momentum in the collinear factorization formalism ($p_\perp = q_\perp = 0$). Then, the momentum fractions are given by $x_1 = \frac{2p_z}{\sqrt{s}}$ and $x_2 = \frac{2q_z}{\sqrt{s}}$ and we can write the four-momenta as

$$p = \left(\frac{x_1\sqrt{s}}{2}, 0, 0, \frac{x_1\sqrt{s}}{2}\right) \text{ and } q = \left(\frac{x_2\sqrt{s}}{2}, 0, 0, -\frac{x_2\sqrt{s}}{2}\right). \tag{B5}$$

Using the expression for the matrix element and integrating the longitudinal components with the δ functions, the cross section becomes

$$\begin{aligned} &(2\pi)^3 2E_k \frac{d\sigma^{pp\to f_2X}}{d^3k} \\ &= \frac{2\pi^2 M^2}{(N_c^2-1)\kappa^2 s}(2\pi)^2\delta^2(k_\perp)G(x_+,Q^2)G(x_-,Q^2). \end{aligned} \tag{B6}$$

The exact same equation was obtained by computing the collinear limit of $k_\perp$ factorization, Eq. (19). Similar results were obtained for η'-meson production [11].

[1] J. C. Collins and R. K. Ellis, Nucl. Phys. **B360**, 3 (1991).
[2] S. Catani, M. Ciafaloni, and F. Hautmann, Nucl. Phys. **B366**, 135 (1991).
[3] L. V. Gribov, E. M. Levin, and M. G. Ryskin, Phys. Rep. **100**, 1 (1983).
[4] E. A. Kuraev, L. N. Lipatov, and V. S. Fadin, Sov. Phys. JETP **45**, 199 (1977) [Zh. Eksp. Teor. Fiz. **72**, 377 (1977)].
[5] H. Jung, Phys. Rev. D **65**, 034015 (2002).
[6] A. V. Lipatov, V. A. Saleev, and N. P. Zotov, arXiv:hep-ph/0112114.
[7] N. P. Zotov, A. V. Lipatov, and V. A. Saleev, Phys. At. Nucl. **66**, 755 (2003).
[8] A. V. Lipatov and N. P. Zotov, Eur. Phys. J. C **44**, 559 (2005) [arXiv:hep-ph/0501172].
[9] B. Andersson *et al*. (Small x Collaboration), Eur. Phys. J. C **25**, 77 (2002).
[10] R. Brock *et al*. (CTEQ Collaboration), Rev. Mod. Phys. **67**, 157 (1995).
[11] J. Jalilian-Marian and S. Jeon, Phys. Rev. C **65**, 065201 (2002).
[12] L. D. McLerran and R. Venugopalan, Phys. Rev. D **49**, 3352 (1994).
[13] L. D. McLerran and R. Venugopalan, Phys. Rev. D **49**, 2233 (1994).
[14] E. Iancu, A. Leonidov, and L. McLerran, arXiv:hep-ph/0202270.
[15] E. Iancu and R. Venugopalan, arXiv:hep-ph/0303204.
[16] R. Venugopalan, arXiv:hep-ph/0412396.
[17] F. Gelis and R. Venugopalan, Phys. Rev. D **69**, 014019 (2004).
[18] M. Gyulassy and L. D. McLerran, Phys. Rev. C **56**, 2219 (1997).
[19] Y. V. Kovchegov and D. H. Rischke, Phys. Rev. C **56**, 1084 (1997).
[20] W. M. Yao *et al*. [Particle Data Group], J. Phys. G **33**, 1 (2006).
[21] C.-K. Chow and S.-J. Rey, J. High-Energy Phys. 05 (**1998**) 010.
[22] C.-K. Chow and S.-J. Rey, Nucl. Phys. B **528**, 303 (1998).
[23] D. Toublan, Phys. Rev. D **53**, 6602 (1996)
[24] F. Giacosa, T. Gutsche, V. E. Lyubovitskij, and A. Faessler, Phys. Rev. D **72**, 114021 (2005).
[25] B. Renner, Phys. Lett. **B33**, 599 (1970).
[26] B. Renner, Nucl. Phys. **B30**, 634 (1971).
[27] W. Gampp and H. Genz, Phys. Lett. **B76**, 319 (1978).
[28] W. Gampp and H. Genz, Phys. Lett. **B79**, 267 (1978).
[29] W. Gampp and H. Genz, Z. Phys. C **1**, 199 (1979).
[30] K. Bongardt, W. Gampp, and H. Genz, Z. Phys. C **3**, 233 (1980).
[31] H. Genz, Phys. Rev. D **26**, 3108 (1982).
[32] K. Ishikawa, I. Tanaka, K. F. Liu, and B. A. Li, Phys. Rev. D **37**, 3216 (1988).
[33] H. Terazawa, Phys. Lett. **B246**, 503 (1990).
[34] M. Suzuki, Phys. Rev. D **47**, 1043 (1993).
[35] Y. Yan and R. Tegen, Phys. Rev. C **54**, 1441 (1996).
[36] E. Katz, A. Lewandowski, and M. D. Schwartz, Phys. Rev. D **74**, 086004 (2006).
[37] J. Adams *et al*. (STAR Collaboration), Phys. Rev. Lett. **92**, 092301 (2004).
[38] G. F. Giudice, R. Rattazzi, and J. D. Wells, Nucl. Phys. **B544**, 3 (1999).
[39] T. Han, J. D. Lykken, and R. J. Zhang, Phys. Rev. D **59**, 105006 (1999).
[40] C. Itzykson and J. B. Zuber, *Quantum Field Theory* (McGraw-Hill, New York, 1980), p. 705.
[41] A. J. Baltz, F. Gelis, L. D. McLerran, and A. Peshier, Nucl. Phys. **A695**, 395 (2001).
[42] F. Gelis and R. Venugopalan, J. Phys. G **30**, S995 (2004).
[43] J. P. Blaizot, F. Gelis, and R. Venugopalan, Nucl. Phys. **A743**, 13 (2004).
[44] J. P. Blaizot, F. Gelis, and R. Venugopalan, Nucl. Phys. **A743**, 57 (2004).
[45] E. Iancu, A. Leonidov, and L. D. McLerran, Nucl. Phys. **A692**, 583 (2001).
[46] E. Ferreiro, E. Iancu, A. Leonidov, and L. McLerran, Nucl. Phys. **A703**, 489 (2002).
[47] J. Jalilian-Marian, A. Kovner, L. D. McLerran, and H. Weigert, Phys. Rev. D **55**, 5414 (1997).
[48] J. Jalilian-Marian, A. Kovner, A. Leonidov, and H. Weigert, Phys. Rev. D **59**, 014014 (1999).
[49] J. Blumlein, arXiv:hep-ph/9506403.
[50] M. Ciafaloni, Nucl. Phys. **B296**, 49 (1988).
[51] S. Catani, F. Fiorani, and G. Marchesini, Nucl. Phys. **B336**, 18 (1990).
[52] S. Catani, F. Fiorani, and G. Marchesini, Phys. Lett. **B234**, 339 (1990).
[53] H. Jung and G. P. Salam, Eur. Phys. J. C **19**, 351 (2001).
[54] M. A. Kimber, A. D. Martin, and M. G. Ryskin, Phys. Rev. D **63**, 114027 (2001).
[55] T. Hahn, Comput. Phys. Commun. **168**, 78 (2005).
[56] M. Hansson and H. Jung, arXiv:0707.4276 [hep-ph].
[57] M. Czech and A. Szczurek, Phys. Rev. C **72**, 015202 (2005).
[58] Y. Zhang, G. I. Fai, G. Papp, G. G. Barnafoldi, and P. Levai, Phys. Rev. C **65**, 034903 (2002).
[59] K. Tuchin, Nucl. Phys. **A798**, 61 (2008).